



Highlights from Telescope Array

YOSHIKI TSUNESADA, FOR THE TELESCOPE ARRAY COLLABORATION

Tokyo Institute of Technology, Meguro, Tokyo 152-8550 Japan

tsunesada@cr.phys.titech.ac.jp

Abstract: The results from the first three years observation in Telescope Array are reviewed. The energy spectrum, mass composition, and anisotropy in arrival directions of ultra-high energy cosmic rays are discussed. The energy spectrum of cosmic rays with energies above 10^{18} eV is determined using the data of the fluorescence detectors, surface detectors, and with a hybrid shower reconstruction technique using the both data. The ankle structure is clearly found at $10^{18.7}$ eV. The second bending point is also identified, at which the flux of cosmic rays begins to decrease and the spectral index changes from $E^{-2.68}$ to $E^{-4.2}$. The study of shower development using the fluorescence detector data shows that proton is dominant in cosmic rays above $10^{18.2}$ eV. No apparent anisotropies in the arrival direction of cosmic rays are found. I also present further experimental extensions which are being developed at the Telescope Array site.

Keywords: Ultra-high energy cosmic rays, Telescope Array, energy spectrum, mass composition, anisotropies

1 Introduction

Telescope Array (TA) is a cosmic ray observatory of the largest exposure in the northern hemisphere, located in the Millard County, 200 km southwest of Salt Lake City, Utah, USA. This is a hybrid experiment by collaborators from Japan, the US, Korea, Russia, and Belgium, using two types of detectors, surface detectors (SDs) and fluorescence detectors (FDs). This can be regarded as a follow-up to the AGASA and HiRes experiments, which used scintillation counters and fluorescence mirrors, to uncover the mysteries of ultra-high energy cosmic rays and to clarify their origin. In this paper, I review the major results from the TA first three years observation, including the energy spectrum, mass composition, and anisotropy of ultra-high energy cosmic rays. The activities for future extensions are also presented.

2 TA detectors

The TA-SD consists of 507 three square meters double-layered scintillation counters in a square grid with 1.2 km separations in a total area of $\sim 700\text{km}^2$ (Figure 1). The average atmospheric depth at the TA ground level is $\sim 860\text{ g/cm}^2$ ($\sim 1400\text{m}$ above the sea level). Signals of shower particles are sampled at 50 MHz frequency and digitized with 12-bit FADC, not integrating all charges from photo-tubes in a $\sim 10\mu\text{s}$ time constant as in conventional air shower array experiments like AGASA. The SD data acquisition system is triggered by a coincidence, within $8\mu\text{s}$ window, of neighbouring three SDs with signals greater than

3 MIPs (minimum-ionizing particles) equivalent in their both layers. The SD array is fully efficient for cosmic rays with energies greater than $10^{18.8}$ eV [2].

The fluorescence detectors are installed in the three stations, those are the Black Rock (BR, 12 telescopes), Long Ridge (LR, 12 telescopes), and Middle Drum (MD, 14 telescopes) sites, viewing the sky above SDs. The 24 BR and LR telescopes were newly developed for TA, and the MD telescopes are refurbished HiRes-1 detectors. One BR/LR telescope is comprised of a cluster of photo-tubes (or a "camera"), and a reflecting mirror of 3.3m diameter. The BR/LR camera has 16×16 2-inch hexagonal tubes covering $15.5^\circ \times 18^\circ$ of the sky. A telescope triggering signal is generated when five adjacent tubes in a camera are fired by incident photons, and waveform data of all the cameras are recorded in a station [3]. The MD telescopes have 5.2m^2 mirrors and cameras of 256 pixels using 40mm Philips tubes. These telescopes are operated with the same electronics and data acquisition system of the HiRes-1 experiment. The total FD fields of view are 108, 108 and 114 degrees in azimuth and $3 \sim 31$ degrees in elevation. See references [1, 4] in this conference for details of the TA detectors.

The TA detectors have been in operation since May 2008. The operational duty cycle of SD is $\sim 98\%$, and the total exposure is $\sim 2,700\text{ [km}^2\text{ str yr]}$ ($\sim 1.7\text{AGASA}$) (\sim April 2011). The telescope on-times are ~ 2400 hours (MD site), which gives $\sim 1/3$ HiRes-1 exposure. The FD duty factor is $\sim 11\%$, and it reduces to $\sim 9\%$ after good weather cut.

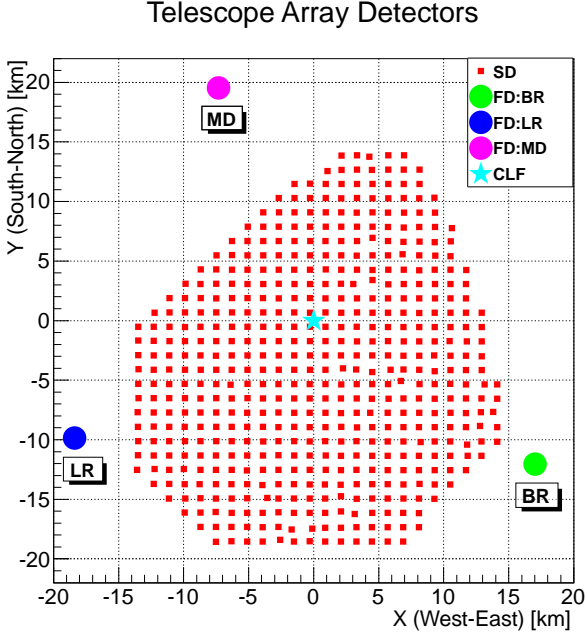


Figure 1: Layout of the TA detectors.

3 Shower analysis

3.1 Shower reconstruction with FD data

The fluorescence detectors measure photons emitted from or around air showers with phototubes exposed to the night sky to determine the longitudinal profiles. The longitudinal profile of an air shower as a function of atmospheric depth X is written by the Gaisser-Hillas function,

$$f(X) = \left(\frac{X - X_0}{X_{\max} - X_0} \right)^{\frac{X_{\max} - X_0}{\lambda}} \exp \left(-\frac{X - X_{\max}}{\lambda} \right) \quad (1)$$

where X_{\max} is the depth at the maximum development of an air shower, X_0 is the first interaction point, λ is a characteristic length of particle interaction. This equation was originally proposed to describe the development of the number of charged particles [5], and is also applicable to an energy deposit profile which can be directly measured with FDs. The *calorimetric energy* of the air shower is obtained by integrating the longitudinal profile,

$$E_{\text{cal}} = N_{\max} \int \left\langle \frac{dE}{dX} \right\rangle f(X) dX = \int \mathcal{E}(X) dX \quad (2)$$

where N_{\max} is the shower size at X_{\max} , $\left\langle \frac{dE}{dX} \right\rangle$ is the mean energy deposit of charged particles per unit length, and $\mathcal{E}(X) \equiv \mathcal{E}_{\max} f(X)$ is the energy deposit profile of the shower. The primary energy of the cosmic ray which induced the shower is obtained from E_{cal} by taking into account the *missing energy* which is an *invisible* component of the shower energy carried away by neutral particles.

The data analysis procedures for the MD data are almost identical to those used in the HiRes experiment [6]. For

the BR/LR data analysis, we have developed new codes suitable for the 10MHz sampling data acquisition system.

Directly calculating the number of charged particles using phototube signal and a given reconstructed air shower geometry is difficult due to the complexities of the FDs, as well as, accounting for the effects of Cherenkov light in the shower. For this reason, an *Inverse Monte Carlo* (IMC) method is employed. Using an IMC method, showers with varying X_{\max} and N_{\max} (or \mathcal{E}_{\max}) are simulated and the number of measured photo-electrons is compared with that produced by the simulated showers. Simulation of the air shower allows for the treatment of Cherenkov radiation and ray-tracing methods are used to understand the acceptance of photons produced on the shower axis. Here we can include all the effects, such as photon shadowing by structures, mirror reflectances, and other calibration-related matters. We use *independently* developed FD simulation/reconstruction programs utilizing the inverse Monte Carlo method. From the differences between energies determined by the two codes, and together with $\sim 5\%$ and $\sim 3\%$ uncertainties which originate from non-predetermined primary nuclear types and the missing energy correction, the energy uncertainty from the reconstruction procedures is evaluated as $\sim 10\%$. Taking into account the systematic uncertainties from FD calibrations [8] or atmospheric effects [9], the total uncertainty in the TA FD energies is $\sim 22\%$ [7].

3.2 Measurement with the surface detector array

Shower particles at the ground level of the TA site are sampled by the SDs with 3 m^2 area. From the lateral distribution of the shower particles determined from the local densities at SDs¹, an energy estimator, S_{800} , the density at 800m from the shower core is evaluated. The lateral distribution function of shower particles we used is an AGASA-type formula [10],

$$\rho(r) \propto \left(\frac{r}{R_M} \right)^{-1.2} \left(1 + \frac{r}{R_M} \right)^{-(\eta-1.2)} \times \left[1 + \left(\frac{r}{1000\text{m}} \right)^2 \right]^{0.6} \quad (3)$$

and the reconstruction procedures are adjusted to fit the TA SD data [11]. In order to take into account different atmospheric attenuation of inclined showers, we construct a lookup table for conversion from the observables ($S_{800}, \sec \theta$) to the energy E_{SD} by using a CORSIKA based Monte Carlo (MC) developed for TA [12, 13, 2] (Figure 2). The SD shower analysis program is tuned to reproduce MC-thrown energies from the estimators ($S_{800}, \sec \theta$) of reconstructed showers.

However, because of the lack of our knowledge of details of ultra-high energy hadronic interactions, there are rather

1. The measured values are not necessarily proportional to number of particles: SDs measure mean energy deposit by shower particles, in terms of vertical muons.

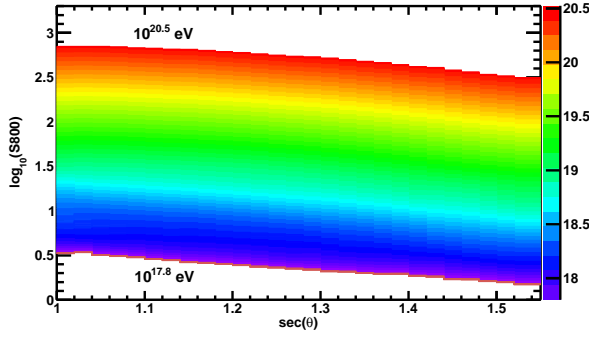


Figure 2: The SD energy chart

large systematic uncertainties in energy determination from the shower particle measurement at the ground compared to the calorimetric measurement by FDs. This is a long-standing problem in cosmic ray physics, and has been discussed in comparisons between AGASA, an SD based experiment, and HiRes, which used FDs. In order to define a "unified" TA energy scale, we use *hybrid* events, which are detected by both SD and either of the three FD sites. From an $E_{SD}^{Hyb} - E_{FD}^{Hyb}$ plot, where E_{SD}^{Hyb} and E_{FD}^{Hyb} are energies determined by the SD and FD reconstruction of the hybrid events respectively, we determined an overall scale factor $\langle E_{FD}^{Hyb} / E_{SD}^{Hyb} \rangle = 1/1.27$ to obtain the energy of each SD event (Figure 3). Therefore the energy of an SD event, which is not necessarily a hybrid event, is given by $E = \langle E_{FD}^{Hyb} / E_{SD}^{Hyb} \rangle E_{SD}$, where E_{SD} is the energy determined from the SD reconstruction [7, 2]. Note that the hybrid events of all the three combinations (SD and either of BR/LR/MD) are plotted in Figure 3. This indicates that the energy scales of all the three FD stations are in consistent even though the entirely different detectors and calibration schemes are used.

4 Energy spectrum

In Figure 4, I show three energy spectra above 10^{18} eV from the TA data analyses, of the MD monocular mode [6], the BR/LR *hybrid* mode [14], and the SD analysis [2]. Here the "BR/LR hybrid" means that we used FD data of BR or LR site, and also the shower particle arrival timing at the position of an SD, which significantly improves the accuracy in determining shower geometries than in the monocular mode [14]. For comparison, the AGASA [15], HiRes [16] and the Pierre Auger Observatory (PAO) [17] spectra are also displayed. We stress that all the three TA spectra are in good agreement (note that the SD energy has been scaled by $1/1.27$ matching to the FD energy scale as described in the previous section). It is also important that the MD data, from the refurbished HiRes-1 detectors, analyzed with the identical procedures used in HiRes, is fully consistent with the HiRes-1 and HiRes-2 results.

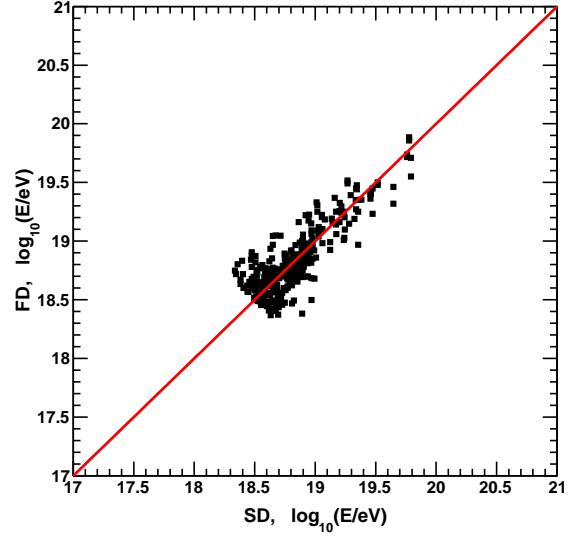


Figure 3: Scatter plot of the energies determined from SD and FD reconstructions using the TA hybrid events. Events of all the three combinations (SD-BR/LR/MD) are plotted.

$A [m^{-2} str^{-1} s^{-1} eV^{-1}]$	$\log_{10}(E_a/eV)$	$\log_{10}(E_c/eV)$
$(2.4 \pm 0.1) \times 10^{-30}$	18.69 ± 0.3	19.68 ± 0.9
k	ℓ	m
-3.33 ± 0.4	-2.68 ± 0.4	-4.2 ± 0.7

Table 1: TA-SD spectral parameters

We applied a broken-power-law fit with two bending points to the SD spectrum, which is of the largest exposure in TA,

$$\frac{dI}{dE}(E) = A \times \begin{cases} E^k, & (E < E_a) \\ E_a^{\ell-k} E^\ell, & (E_a \leq E < E_c) \\ E_a^{\ell-k} E_c^{\ell-m} E^m, & (E > E_c) \end{cases} \quad (4)$$

where k, ℓ, m are spectral indices, E_a, E_c are the bending points, and A is a normalization constant. The fit parameters are listed in Table 1. The "ankle" structure is found at $\log_{10}(E_a/eV) = 18.69$, and the second bending point is also identified at $\log_{10}(E_c/eV) = 19.68$. The number of events observed above E_c is $N_{obs} = 28$, while expected $N_{exp} = 54.9$ in an absence of the second bend. The significance of the event deficit above the "cut-off" energy E_c is evaluated as $\sum_{i=0}^{28} \text{Poisson}(\mu = 54.9; i) = 4.75 \times 10^{-1} \sim 3.9\sigma$.

5 Mass composition

The information on the primary nuclear types of cosmic rays can be obtained from the longitudinal developments of air showers initiated by them. The fluorescence detector is a powerful tool for this purpose, since it measures

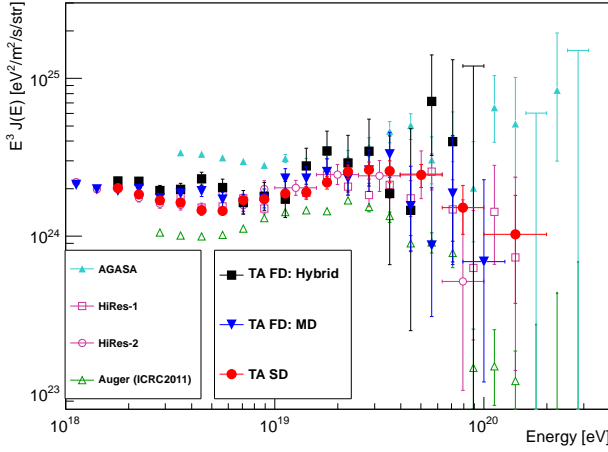


Figure 4: TA energy spectra from SD (filled circle), FD mono (MD site, filled triangle), and BR/LR hybrid (filled square).

shower profiles at different atmospheric depths with many photo-tube "pixels". Here we used BR/LR *stereo* events, which were detected at the two sites, because their shower geometries can be determined more accurately than in case of the monocular mode. We used X_{\max} , the maximum development point of an air shower, as the mass indicator: X_{\max} is larger (deeper in the atmosphere, lower altitudes) for protons or lighter nuclei, and smaller (higher altitudes) for heavier nuclei as iron. We compared the distribution of X_{\max} of observed showers and those predicted from a shower Monte-Carlo using the CORSIKA code [12]. A caveat should be made here: since we observe cosmic rays at the fixed ground levels with the limited field of view, the distribution of observed X_{\max} should be different from a prediction by a shower generator like CORSIKA even if the primary composition is fully known, unless applying a sophisticated data selection ². We take another approach here. We use a "standard" data selection rule for the stereo events. Instead of finding a special selection filter for the data, we apply our detector and triggering simulation, and also the selection criteria to the CORSIKA showers exactly same as to the data [19]. The distributions of X_{\max} of such Monte-Carlo showers with the detector simulation and the cuts can be compared with those of the real data.

The distributions of X_{\max} of the observed showers for different energy regions in $E = 10^{18.4 \sim 19.6}$ eV are shown in Figure 5 [20]. The expected distributions for pure-proton and pure-iron primaries are also shown, obtained from our Monte-Carlo studies using the CORSIKA showers with the TA-FD detector simulations and the same data cuts. In order to examine the compatibilities of the observed X_{\max} and the predictions, KS tests were carried out calculating the "p-values" as functions of energies. Here we used CORSIKA shower libraries of three different hadronic interaction models, QGSJET-01, QGSJET-II, and Sibyll. In

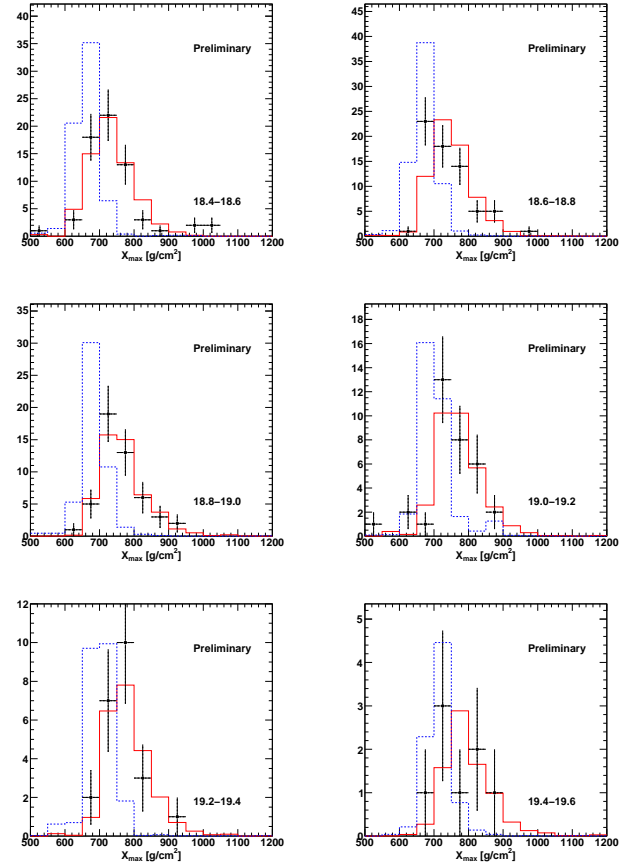


Figure 5: X_{\max} distributions of the observed showers of the different energy regions (markers), together with the expected ones predicted from our Monte-Carlo studies using CORSIKA showers with the TA-FD detector simulations (histograms: solid for protons and dashed for iron nuclei). The QGSJET-II hadronic interaction model is used.

all the energies and the hadronic interaction assumptions, the TA data are compatible with the proton primary predictions. In the higher energies ($E > 10^{19.4}$ eV), the p-values are also high for the iron hypothesis, but the statistics are still limited.

I show the averaged X_{\max} as a function of energy in Figure 6 [20]. One can see again that the TA data is consistent with the proton-dominated composition of ultra-high energy cosmic rays. Note that the proton and iron primary prediction lines in Figure 6 are also obtained by applying the TA detector simulation and the same data cuts for the data, therefore both the data and the prediction lines in this figure cannot be directly compared with the results from other experiments, like HiRes or PAO.

2. The PAO uses well-tuned data cuts which give a "true" X_{\max} distribution from the observed data [18].

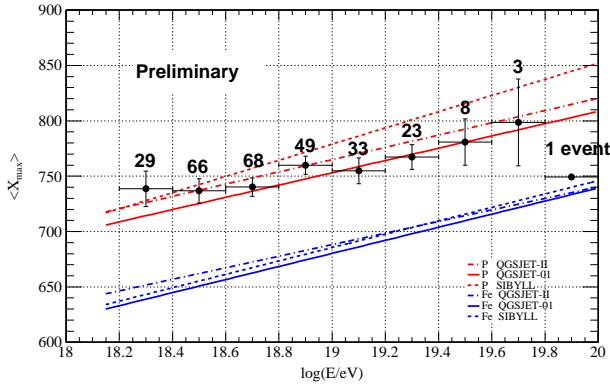


Figure 6: $\langle X_{\max} \rangle$ plot as a function of energy. The proton and iron prediction lines are obtained through the TA-FD detector simulation and the cuts exactly same for the data.

6 Anisotropies

The major difficulty in exploring the origin of cosmic rays is the magnetic deflections of charged particle trajectories from their sources to the Earth. However, *anisotropies* in the cosmic ray arrival direction distribution still give important clues, by finding hot spots of cosmic rays or correlations with possible source populations. We used the TA-SD events collected from May 2008 to April 2011, of zenith angles smaller than 45° and angular accuracies $\sim 1.5^\circ$. Note that the SD event energies have been renormalized to the FD energy scale ($1/1.27$) as described in the Section 3.2. The data set contains 854 events with energies greater than 10EeV , and 49, 20 for $E > 40\text{EeV}$, $> 57\text{EeV}$, respectively.

First we examined auto-correlation of the TA events, or event clusterings as reported by the AGASA group [21], without making any assumptions on cosmic ray sources. The number of event pairs in a given angular window δ is counted, and calculated a probability $P(\delta)$ that the uniform distribution of cosmic rays yields the same or a greater number of pairs by chance than the observed one. The result is shown in Figure 7 as a function of the window size [22]. There is a rather small $P(\delta)$ region around the angular scale $\delta \sim 15^\circ$ for $E > 57\text{EeV}$, but not statistically significant to support a deviation from the isotropy.

Second, we searched for cross-correlation of the TA events and active galactic nuclei (AGN), which have been considered as possible cosmic ray production sites. The procedures and parameters used in this analysis are similar to those used in the studies by PAO [24]. We consider AGNs, QSOs and BL Lacs in the object catalog (the Veron-Cetty & Veron (VCV) catalog [23]) with redshift smaller than 0.018, and search for correlation with the TA events of $E > 57\text{EeV}$ (20 events) within an angular separation of 3.1° (Figure 8). We assumed that all the objects have the same intrinsic cosmic ray intensities regardless of class or distance. The number of TA events correlating with the

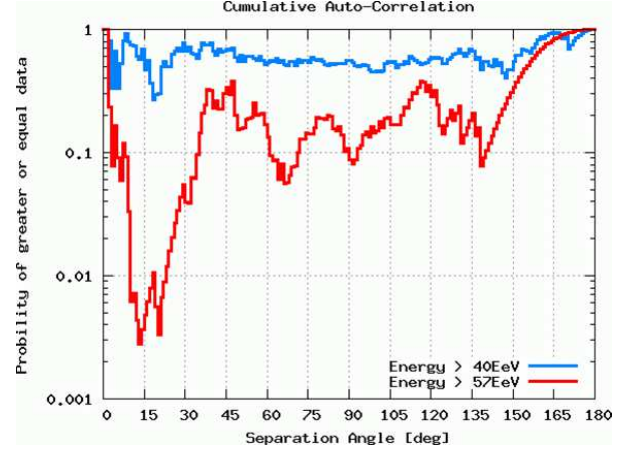


Figure 7: Auto-correlation analysis: the vertical axis is probability that the uniform distribution of cosmic rays accidentally gives the same or a greater number of event pairs than the observed number of pairs in a given angular separation.

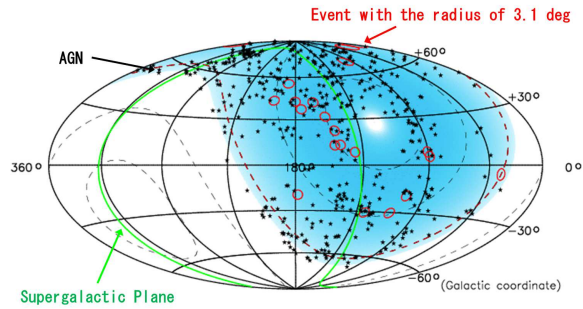


Figure 8: 20 TA events of $E > 57\text{EeV}$ and the AGN in the VCV catalog [23]. Galactic coordinates.

VCV AGN is shown in Figure 9, as a function of the total number of events with energies greater than 57EeV , in an order of the detection date [22]. We found 8 correlated events out of 20, while we expect 5 (25%) chance correlation if the source distribution were isotropic in the TA sky. The statistical significance of a deviation from the isotropy is also small in this analysis, therefore the AGN hypothesis on the cosmic ray origin is not supported by the present TA data.

Lastly we investigated a correlation between the TA events and matter distribution in the universe. We employ the flux sampling method developed in [25], and previously applied to the HiRes data [26]. We use 109,408 objects from the 2MASS Galaxy Redshift Catalog (XSCz) [27], which are located at distances $5 < d < 250\text{Mpc}$ from the Earth, as tracers of the local matters in the large-scale structure (LSS) of the universe. The expected cosmic ray density map is constructed as a superposition of the contributions of the individual galaxies, taking into account an angular spreading (or *smearing*) as a result of the magnetic deflections by the extra-galactic and Galactic irregular fields, flux

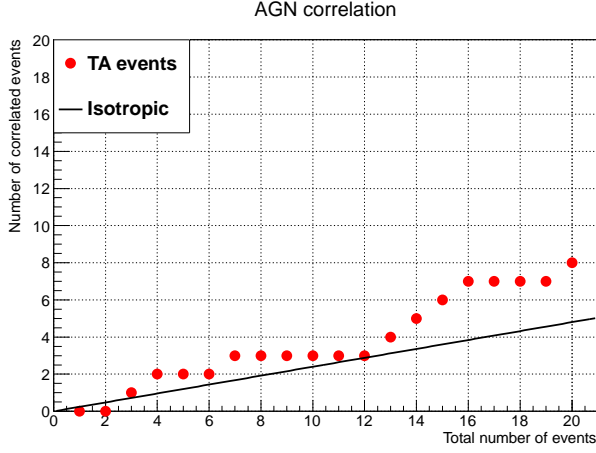


Figure 9: The growth of the number of TA events ($E > 57$ EeV) correlating with AGN since 2008.

attenuations due to cosmic ray interactions (e.g. photo-pion productions, e^\pm pair productions), and the TA exposure. Here the smearing effect is simply introduced as a Gaussian spreading with the smearing angle θ_s . The uniform component of cosmic rays, as cumulative contribution of sources beyond 250 Mpc, is also added. We assume that all the primary cosmic rays are protons, in accordance with the TA composition study [19, 20]. The obtained flux maps for $E > 10$, > 40 , and > 57 EeV, together with the TA events, are shown in Figure 10. The compatibilities of the LSS hypothesis or the isotropy with the TA events were examined with the KS test. The p-values as a function of the smearing angle are shown in Figure 11 for the structure hypothesis, as well as for the isotropic distribution [28, 29]. The TA data of $E > 10$ EeV is isotropic, and not compatible with the structure hypothesis. The p-values for $E > 40$ and > 57 EeV are rather higher, but there are no significant differences between the structure and isotropy hypotheses. If we consider regular components of the Galactic magnetic field, including a halo and a disk fields, the p-values of the structure model is mildly increased, while the compatibility with the isotropy is also maintained. Therefore we conclude that there are no convincing evidences of correlations with any classes of source candidates in the present TA data.

7 Further developments

There are several sources of energy uncertainties in the fluorescence measurements, as atmospheric effects and fluorescence yields. There have been remarkable progress in laboratory measurements on fluorescence yields, however, it is not straightforward to apply the results to an actual cosmic ray experiment taking into account all the atmospheric conditions. An *in situ* measurement of fluorescence light using known charged particle energies is of great advantage in a cosmic ray experiment, and the Electron Light Source

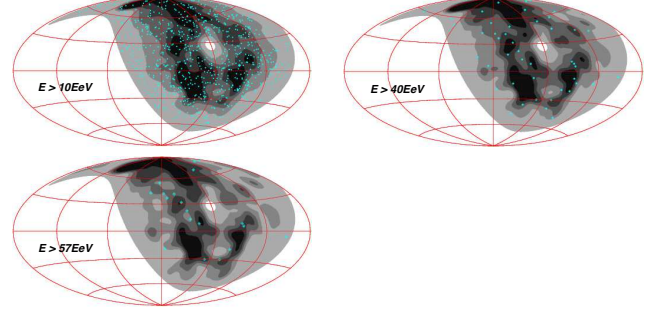


Figure 10: The expected cosmic ray density map obtained from the algorithm in [25] with the smearing angle $\theta_s = 6^\circ$ (contours). The dots are the TA events of the corresponding energies. Galactic coordinates ($\ell = 0$ at the right edge of the figure, increasing ℓ to the left, 180° at the center, and 360° at the left edge).

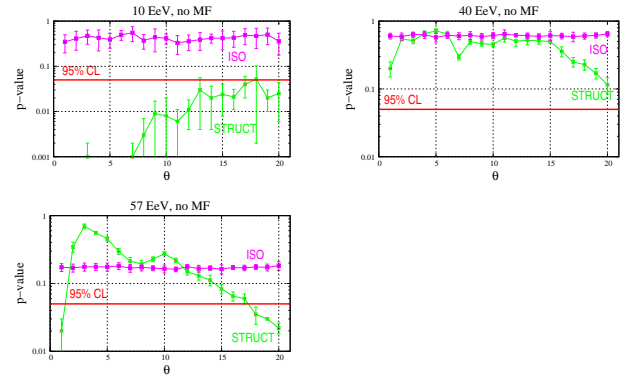


Figure 11: The KS test results for the compatibilities between the hypotheses (structure and isotropy) and the TA data. No regular component of the Galactic magnetic field is considered. The horizontal line shows an *a priori* chosen confidence level of 95%.

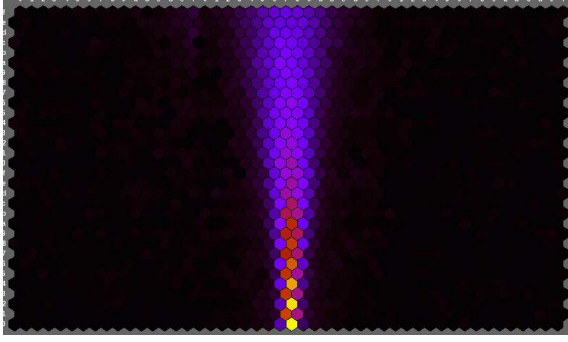


Figure 12: An example of the ELS beam shot seen from the TA fluorescence detectors.

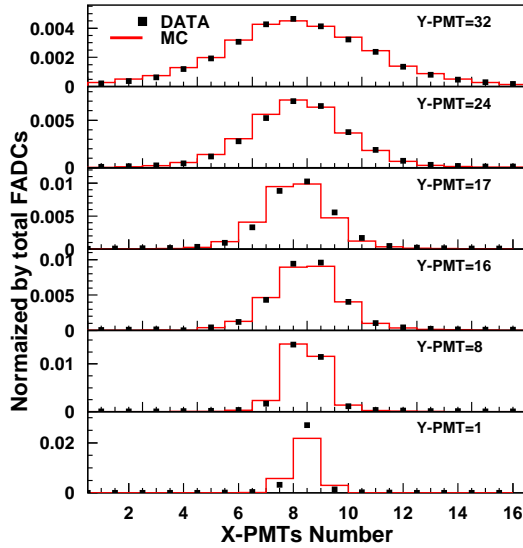


Figure 13: Photo-tube signals obtained from an ELS trigger of the fluorescence detectors.

(ELS) of TA is the unique one for this purpose [31]. This 40 MeV electron shooter has been installed at the Black Rock site, 100m away in front of the fluorescence detectors, which enables us an end-to-end calibration of our detectors, atmospheric effects, and also fluorescence yields. The ELS has been operational since September 2010 (a beam shot example is shown in Figure 12). The signals (waveforms) obtained by the photo-tubes which see the electron beams from ELS are shown in 13, which are in good agreement with our Monte-Carlo expectations [31]. The analysis of the ELS data is now ongoing, in order to reduce the systematic uncertainty in the FD energies by $\sim 10\%$.

I introduce two experimental activities under development in TA. The one is the TA Low-energy Extension (TALE) [32]. Precise measurements of energy spectrum and mass composition of cosmic rays at energies $10^{17} \sim 10^{18}$ are

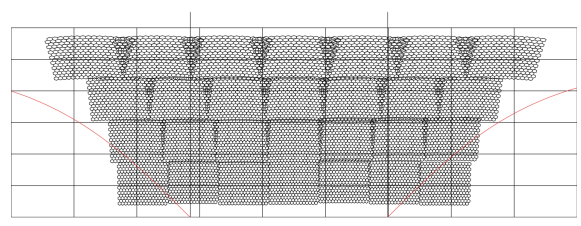


Figure 14: TALE-FD field of view

quite important by several reasons. In particular, a possible transition of cosmic rays of Galactic sources to those of extra-galactic origins is of special interest. There is a general agreement that heavier nuclei are dominant in cosmic rays around the knee region ($E = 10^{15 \sim 16}$ eV), and the average mass increases with energy up to $\sim 10^{17}$ eV. This is consistent with the supernova-origin scenario of cosmic ray production and acceleration in our Galaxy. On the other hand, there are several experimental results which suggest proton dominant composition above 10^{18} eV [33]. Therefore it is expected that there could be a drastic change in mass composition of cosmic rays at $10^{17 \sim 18}$ eV, which gives a crucial experimental constraint on astrophysical interpretations of the proposed *second knee* or the ankle structures in the energy spectrum. TALE is designed to lower the minimum detection energy of TA by about an order of magnitude, with the hybrid detection technique. Reconditioned HiRes-2 detectors as the TALE FD will be installed in the immediate vicinity of the MD site i.e. the HiRes-1 detectors. The TA-TALE FD covers from 3° to 59° in elevation (Figure 14), which enable us to detect lower energy cosmic rays and a bias-free X_{\max} measurement. An infill array is being installed in front of the TA-TALE FDs. A sub-array of 45 counters with a spacing of 400m at a distance of 1.5 km from the TALE-FD gives a 10% efficiency for cosmic rays at 3×10^{16} eV. In order to cover more area, we change the spacing to 600 in a range of $3 \sim 5$ km from the FD. For larger distances we use the spacing of the main TA SD array, 1200 m. The layout of the TALE SD is shown in Figure 15.

The another experimental extension in TA is a *bistatic radar* detection of ultra-high energy cosmic rays (TARA) [34, 35], firstly explored by the MARIACHI project [36]. This is a lower-cost, 24 hour duty cycle remote sensing technique for the next generation cosmic ray observatories. An important advantage of the bistatic radar technique among the several radio detection methods proposed for cosmic rays comes from the fact that the scattering cross-section is largest in the forward direction [37]: a radio pulse sent from the transmitter station, and reflected by air shower plasma can be effectively detected at the receiver station. The signal of the reflected radio pulse has a "chirp" waveform due to a Doppler-like effect by the scatterer, which is the unique feature of the air shower echoes. We have installed a 2 kW analog television transmitter donated from KUTV Channel 2 in Salt Lake City (Figure 16).

0 2 4 6 8 10 12 14 16

0 2 4 6 8 10 12 14 16

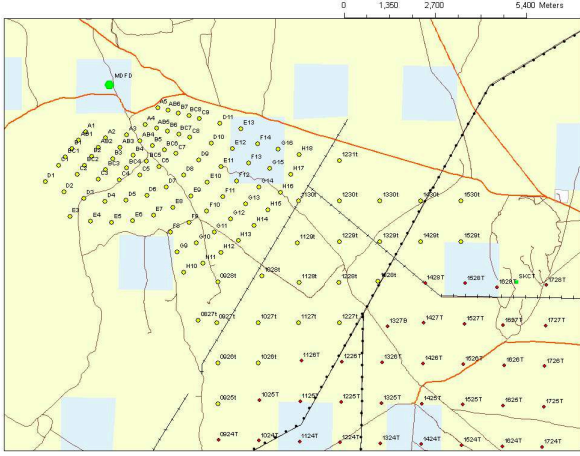


Figure 15: Layout of the TALE infill array. The light-colored circles indicated with "A"-H" or 4 digits + "t" are the TALE counters to be added [32]. The other darker circles with 4 digits + "T" represent the existing counters in the north-west part of the TA SD [1].

This was commissioned in January 2011, operated at a single carrier frequency at 54.1 MHz. The receiver antennas have been deployed at the TA-LR site, 50 away from the transmitter station (Figure 16, 17). We also plan to utilize the radar transmitter in conjunction with the TA ELS. The transmitter will be upgraded at least to 40 kW by the support from the US-NSF/MRI.

8 Discussion

There is a $\sim 20\%$ energy scale difference between TA and PAO, as inferred from the energy spectra. It should be noted that there are $22 \sim 23\%$ systematic uncertainties in energy determinations in both experiments, therefore it is

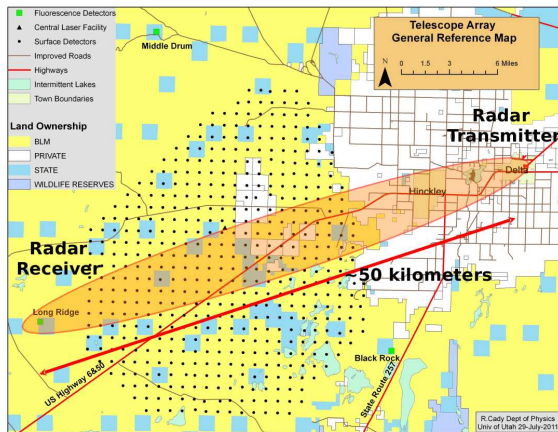


Figure 16: TA bistatic radar (TARA): the radio transmitter and the receiver have been installed at a distance of 50 km.



Figure 17: TA radar receiver

possible to say that the two results are consistent within the systematic errors. However, the 20% difference is not negligible and cannot be overlooked for better understanding of air shower experiment and astrophysics of cosmic rays. It is partly attributed to the different fluorescence yield models employed in the two groups ($\sim 10\%$), but not fully explained only with it. Some cross-calibration of the detectors will be required to reduce the energy scale difference, e.g. exchanging the calibration tools or using the TA ELS (this is the author's personal opinion, and it has not been officially discussed yet between the group headquarters).

Both the TA and PAO $\langle X_{\max} \rangle$ results show that proton is dominant at energies above $10^{18.2}$ eV. It can be interpreted that we have not observed an increase of average mass of cosmic rays in the lower energies, which is expected from the results of the air shower array experiments targeted at and above the knee region. This indicates the importance of the lower energy extensions like TA-TALE [32], or AMIGA and HEAT in PAO [38]. It is controversial that there is an apparent difference in the composition studies in TA and PAO in higher energies. The TA $\langle X_{\max} \rangle$ result is consistent with a proton-dominant composition of cosmic rays [20] (there is one event with a rather smaller $\langle X_{\max} \rangle$ at the highest energy bin, but it is of essentially no significance), but an increase of average cosmic ray mass has been suggested from the PAO data (e.g. [18, 39, 40]). I propose that we try the same analysis procedures: now we are developing a bias-free data cut and determining $\langle X_{\max} \rangle$ as carried out in PAO (our preliminary result shows that this brings same amount of shifts in $\langle X_{\max} \rangle$ to both the data and Monte-Carlo, therefore the conclusion of proton-dominant composition is not changed at all.). It is possible to employ the TA-style analysis given in [19, 20] in PAO. It is also important to revisit the high-energy hadronic interaction models, after the recent experimental progress by LHC [41].

In 2007, the PAO claimed that the distribution of cosmic ray arrival directions is not isotropic and suggested a possible correlation with AGN [42]. However, the statistical significance of the AGN hypothesis in the PAO data has been decreased in their updated analysis [43, 40]. The current TA data shows no statistically significant small or large-scale anisotropies. Unfortunately the interesting region around Cen A is out of the TA sky. There is no hot spot around the Virgo cluster in the TA data. The absence of apparent anisotropy or correlation with known astronomical objects could bring a difficulty in the interpretation of the spectral features, in particular of the steepening at $\sim 5 \times 10^{19}$ eV, firstly claimed by the HiRes experiment [44], and also found in PAO [45] and TA [2]. If the primary cosmic rays are protons, and the steepening is due to cosmic ray energy losses through interaction with the cosmic microwave background photons (the Greisen-Zatsepin-Kuzmin effect [46]). If this is the case there could exist a cosmic ray "horizon" at a certain distance from the Earth, and hence a strong correlation with nearby objects. Another interpretation is that a heavier component is dominant at the highest energies, therefore the steepening we observed is not due to the GZK effect, but to other processes, e.g. acceleration limit at production sites. In any case, no consistent picture of cosmic ray nature can be drawn from the current observation data, although we believe that we are just about the answer. Further efforts in data analysis are required in determining energies and composition, and statistics for anisotropy studies.

9 Conclusions

Telescope Array is the largest cosmic ray observatory in the northern hemisphere, which has been operational in full configuration since May 2008. The TA exposure is ~ 1.7 AGASA in SD, and $\sim 1/3$ HiRes in FD. We have developed detector simulators and shower reconstruction programs for both SD and FD, and the distributions of the observed data are in excellent agreement with expectations using a previously measured spectrum of cosmic rays. The energy scales of the three FD stations (BR, LR and MD sites) are also in agreement, even though different detectors and calibration schemes are used.

I presented the major results from the recent progress of the TA science, including the energy spectrum, mass composition, and anisotropy of ultra-high energy cosmic rays. The energy spectrum of cosmic rays has been derived from analyses of the FD, SD, and the hybrid data. All of the three spectra are in good agreement. From the spectral fit of the SD spectrum, which is of the largest exposure in TA, we found the ankle structure at $10^{18.69}$ eV. We also identified a steepening in the spectrum at $10^{19.68}$ eV with a change of the spectral index from -2.68 to -4.2 . An extended spectrum of cosmic rays at the highest energies is ruled out by a statistical significance of 3.9σ . We studied the distribution of X_{\max} , at which an air shower has its maximum size, using the FD data. We compared to the X_{\max} distribution

of the data and expectations from proton or iron nuclei primaries. The TA data is consistent with the proton-dominant composition. Furthermore, we examined the arrival directions of cosmic rays with energies greater than 10 EeV, and searched for anisotropies or correlations with known astronomical objects. We concluded that no statistically significant anisotropies are found in the present TA data. I introduced a challenge for an end-to-end calibration of the FDs using the electron accelerator (ELS). I also discussed the further experimental developments in near future, the TA low energy extension (TALE), and the bistatic radar detection of ultra-high energy cosmic rays with TARA.

It will have been 100 years in 2012 since the discovery of cosmic rays by Victor Hess. The world financial and political clock is ticking. A critical question to cosmic ray physics is that : "who knows we would discover the origin of cosmic rays?" If the TA energy measurement and the composition study are correct, the final unsolved problem is anisotropy. Our study shows that the statistical power of distinguishing different hypothesis on cosmic ray origins are still weak, and smaller than 50% in the current TA data [28]. This will be significantly improved if we have statistics doubled or tripled, therefore we need observations several more years. We'll also have to discuss the next generation cosmic ray observatory with a huge coverage, to explore the astronomy by charged particles.

Acknowledgement

The Telescope Array experiment is supported by the Japan Society for the Promotion of Science through Grants-in-Aid for Scientific Research on Specially Promoted Research (21000002) "Extreme Phenomena in the Universe Explored by Highest Energy Cosmic Rays", and the Inter-University Research Program of the Institute for Cosmic Ray Research; by the U.S. National Science Foundation awards PHY-0307098, PHY-0601915, PHY-0703893, PHY-0758342, and PHY-0848320 (Utah) and PHY-0649681 (Rutgers); by the National Research Foundation of Korea (2006-0050031, 2007-0056005, 2007-0093860, 2010-0011378, 2010-0028071, R32-10130); by the Russian Academy of Sciences, RFBR grants 10-02-01406a and 11-02-01528a (INR), IISN project No. 4.4509.10 and Belgian Science Policy under IUAP VI/11 (ULB). The foundations of Dr. Ezekiel R. and Edna Wattis Dumke, Willard L. Eccles and the George S. and Dolores Dore Eccles all helped with generous donations. The State of Utah supported the project through its Economic Development Board, and the University of Utah through the Office of the Vice President for Research. The experimental site became available through the cooperation of the Utah School and Institutional Trust Lands Administration (SITLA), U.S. Bureau of Land Management and the U.S. Air Force. We also wish to thank the people and the officials of Millard County, Utah, for their steadfast and warm support. We gratefully acknowledge the contributions from the technical staffs of our home institutions and

the University of Utah Center for High Performance Computing (CHPC).

References

- [1] T. Nonaka *et al.*, *Proc. 32nd ICRC*, **0984** (2011) (this conference);
- [2] D. Ivanov, B.T. Stokes *et al.*, *Proc. 32nd ICRC*, **1297** (2011) (this conference)
- [3] Y. Tameda *et al.*, *Nucl., Instr. Meth. A*, **609**, 227 (2009)
- [4] S. Ogio *et al.*, *Proc. 32nd ICRC*, **1308** (2011) (this conference)
- [5] T.K. Gaisser and A.M. Hillas, in *Proc. 15th ICRC*, **8**, 353 (1977)
- [6] D. Rodriguez *et al.*, *Proc. 32nd ICRC*, **1303** (2011) (this conference)
- [7] T. Abu-Zayyad *et al.*, *Proc. 32nd ICRC*, **1270** (2011) (this conference)
- [8] H. Tokuno *et al.*, *Nucl., Instr. Meth. A*, **601**, 364 (2009)
- [9] T. Tomida *et al.*, *Nucl., Instr. Meth. A*, **654**, 653 (2011)
- [10] K. Shinozaki and M. Teshima [AGASA Collaboration], *Nucl. Phys. Proc. Suppl.*, **136**, 18 (2004)
- [11] G.B. Thomson, *PoS ICHEP2010* (2010) 448 [arXiv:1010.5528 [astro-ph.HE]]
- [12] D. Heck, G. Schatz, T. Thouw, J. Knapp, and J.N. Capdevielle, *CORSIKA: A Monte Carlo code to simulate extensive air showers*, (1998), Technical Report 6019, FZKA.
- [13] B.T. Stokes *et al.*, *Proc. 32nd ICRC*, **1288** (2011) (this conference)
- [14] D. Ikeda *et al.*, *Proc. 32nd ICRC*, **1264** (2011) (this conference)
- [15] M. Takeda *et al.*, *Phys. Rev. Lett.*, **81**, 1163 (1998), M. Takeda *et al.*, *Astropart. Phys.*, **19**, 447 (2003)
- [16] R.U. Abbasi *et al.*, *Phys. Rev. Lett.*, **100**, 101101 (2008)
- [17] The Pierre Auger Collaboration, *Proc. 32nd ICRC* (2011) (this conference, arXiv 1107.4809)
- [18] J. Abraham *et al.*, *Phys. Rev. Lett.*, **104**, 091101 (2010)
- [19] Y. Tameda *Proc. of UHECR2010 Nagoya Conference* (AIP Conference Proceedings Series, Volume 1367, page 110, in press)
- [20] Y. Tameda *et al.*, *Proc. 32nd ICRC*, **1268** (2011) (this conference)
- [21] N. Hayashida *et al.*, *Phys. Rev. Lett.*, **77**, 1000 (1996)
- [22] I. Tkachev, T. Okuda *et al.*, *Proc. 32nd ICRC*, **1311** (2011) (this conference)
- [23] M.P. Veron-Cetty, and P. Veron, *Astron. Astrophys.*, **455**, 773-777 (2006)
- [24] J. Abraham *et al.*, *Science*, **318**, 938-943 (2007), *Astropart. Phys.* **29**, 188-204 (2008), *Astropart. Phys.* **34**, 314-326 (2010)
- [25] H.B.J. Koers and P. Tinyakov, *JCAP*, **0904**, 003 (2009), *Mon. Not. Roy. Astron. Soc.*, **399**, 1005-1011 (2009)
- [26] R.U. Abbasi *et al.*, *Astrophys. J. Lett.*, **713** L64?L68 (2010)
- [27] We thank T. Jarrett for providing us with the preliminary version of this catalog.
- [28] P. Tinyakov *et al.*, *Proc. of UHECR2010 Nagoya Conference* (AIP Conference Proceedings Series, Volume 1367, page 100, in press)
- [29] P. Tinyakov, E. Kido *et al.*, *Proc. 32nd ICRC*, **1317** (2011) (this conference)
- [30] T. Shibata *et al.*, *Nucl., Instr. Meth. A*, **597**, 61 (2008), *Proc. of UHECR2010 Nagoya Conference* (AIP Conference Proceedings Series, Volume 1367, page 44, in press)
- [31] T. Shibata *et al.*, *Proc. 32nd ICRC*, **1252** (2011) (this conference)
- [32] T. Shibata *et al.*, *Proc. 32nd ICRC*, **1307** (2011) (this conference)
- [33] For example: T. Abu-Zayyad *et al.*, *Astrophys. J.*, **557**, 686 (2001), R. Abbasi *et al.*, *Phys. Rev. Lett.*, **104**, 161101 (2010)
- [34] J. Belz *et al.*, *Proc. of UHECR2010 Nagoya Conference* (AIP Conference Proceedings Series, Volume 1367, page 144, in press)
- [35] C. Allen, J. Belz *et al.*, *Proc. 32nd ICRC*, **1314** (2011) (this conference)
- [36] <http://www-mariachi.physics.sunysb.edu/>
- [37] N.J. Willis, *Bistatic Radar*, Scitech Publishing (1995)
- [38] F. Sánchez *et al.*, *Proc. 32nd ICRC*, **0742** (2011) (this conference), T.H.J. Mathes *et al.*, *Proc. 32nd ICRC*, **0761** (2011) (this conference)
- [39] D. Garcia-Pinto *et al.*, *Proc. 32nd ICRC*, **0709** (2011) (this conference)
- [40] K.H. Kampert, *Recent results from the Pierre Auger Observatory*, *Proc. 32nd ICRC*, (2011) (this conference)
- [41] G. Tonelli, *Results from the experiments at the LHC*, *Proc. 32nd ICRC*, (2011) (this conference)
- [42] The Pierre Auger Collaboration, *Science*, **318**, 938 (2007)
- [43] P. Abreu *et al.*, *Astropart. Phys.*, **34**, 314 (2010), A. Letessier-Selvon, *Proc. of UHECR2010 Nagoya Conference* (AIP Conference Proceedings Series, Volume 1367, page 94, in press)
- [44] R.U. Abbasi *et al.*, *Phys. Rev. Lett.*, **100**, 101101 (2008)
- [45] J. Abraha *et al.*, *Phys. Rev. Lett.*, **101**, 061101 (2008), *Phys. Lett. B*, **685**, 239 (2010)
- [46] K. Greisen, *Phys. Rev. Lett.*, **16**, 748 (1966)